Study of cavities in a creep crack growth test specimen

Available online at www.sciencedirect.com

ScienceDirect

Procedia Structural Integrity 2 (2016) 942–949

Structural Integrity Procedia

www.elsevier.com/locate/procedia

21st European Conference on Fracture, ECF21, 20-24 June 2016, Catania, Italy

Study of cavities in a creep crack growth test specimen

H Jazaeri[a] *, P J Bouchard[a], M T Hutchings[a], A A Mamun[a], R K Heenan[b]

[a]*Department of Engineering and Innovation, Materials Engineering, The Open University, Walton Hall, Milton Keynes, MK7 6AA, UK*
[b]*ISIS Facility, R3 1-22, STFC Rutherford Appleton Laboratory, HSIC, Didcot, OX11 0QX, UK*

Abstract

Small Angle Neutron Scattering (SANS) and Scanning Electron Microscopy (SEM) have been used to determine the degree of cavitation damage, of length scale 5-300 nm, associated with a creep crack grown in a compact tension specimen cut from a Type 316H stainless steel weldment. The specimen was supplied by EDF Energy as part of an extensive study of creep crack growth in the heat affected zone of reactor components. The creep crack propagates along a line 1.5 mm away from, and parallel to, the weld fusion line boundary before deviating away into parent material. The SANS results show a systematic increase in fractional size distribution of cavities approaching the crack, along lines normal to the crack line, and along lines parallel to the crack line approaching the crack mouth. Both SANS and quantitative metallography measurements using SEM indicate two populations of cavities: smaller cavities of less than 100 nm size having a mean diameter of about 60 nm, and a population of larger cavities of 100-300 nm size with a mean diameter of about 200 nm.

Peer-review under responsibility of the Scientific Committee of PCF 2016.

Keywords: Creep crack growth; Cavities; Small Angle Neutron Scattering, Quantitative Metallography

1. Introduction

Strain-relief cracking, also referred to as reheat cracking, is a generic creep failure mode that has been observed in some welded stainless steel structures operating at high temperatures in UK nuclear power plants (Coleman et al., 1998). The cracking is caused by a combination of thermal relaxation of weld residual stress (Turski et al., 2008) and reduction in material creep ductility at the operating temperature. Creep ductility reduces at slower creep deformation rates such as those that occur under power plant operation (Hales, 1983). Although reheat cracking has been studied over the years, a better understanding of the underlying physics and micro-mechanisms contributing to creep damage development is required, with particular attention to cavity nucleation. Indeed, one of the challenges currently faced

Peer review under responsibility of the Scientific Committee of PCF 2016.
10.1016/j.prostr.2016.06.121

by the nuclear utility EDF Energy is the need to predict, with high certainty, the life-time of ageing engineering plant operating in the creep regime.

2. Material

EDF Energy have carried out creep crack growth testing on a compact tension (CT) specimen with the design, geometry, and dimensions as shown in Fig.1. This test specimen, (FD-12), was made of AISI Type 316H austenitic stainless steel material. It was fabricated from a new weldment made by joining two ex-service superheater headers from Hartlepool and Heysham I nuclear power plants. These had plant references HRA1A2/1 and HYA1D2/4, cast No. 55885 and No. 53547, respectively. The former Hartlepool header had been removed from service after an estimated 98,704 hours at a mean temperature of 517°C. A single bevel weld between the header materials was produced in a way that the fusion boundary was perpendicular to the original header wall. A standard 25 mm thick CT specimen was machined from the weldment such that the crack plane was located parallel to, and 1-2 mm, from the weld fusion boundary. Prior to testing by EDF, this specimen was fatigue pre-cracked at room temperature. An isothermal creep crack growth test was then carried out first at 525°C, and subsequently at reduced temperature of 480°C, in order to examine the effects of temperature change. The test was performed on the heat affected zone (HAZ) located in the Hartlepool header side into which the crack grew as shown in Fig. 1.

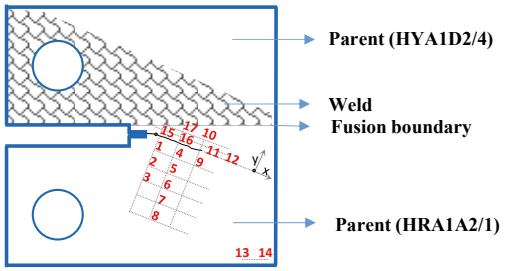

Fig. 1. Schematic illustration of the CT specimen configuration, the crack path and measurement points.

A summary of the creep crack growth data is presented in Table 1. Allport and Dean have reported full details of the tests and creep crack growth rate measurement at EDF (Allport and Dean, 2013). A 3 mm thick slice was removed from the mid-thickness of the CT specimen and used for metallographic examination by AMEC Commercial (Duncombe et al., 2012). This initial metallography examination showed that the creep crack initiated at about 1.5 mm away from the weld fusion boundary, and had deviated away from the weld fusion boundary towards the parent material.

Table 1. Summary of creep crack growth data.

Specimen ID	Material	Temperature (°C)	Duration (h)	Creep crack growth (mm)
FD-12	316 H, welded joint of two ex-service headers (Hartlepool HRA1A2/1 and Heysham I HYA1D2/4)	525	29942	6.37
		480	1676	0.69
			total: 31618	total: 7.06

The 3 mm thick CT section was subsequently examined in more detail by the Open University for the purpose of quantifying the state of creep damage in the region of the crack. The techniques used were Small Angle Neutron Scattering (SANS) and Quantitative Metallography (QM) using Scanning Electron Microscopy (SEM). A 1 mm thick slice was cut from one side of the as-received 3 mm thick specimen using a wire electro-discharge machine (EDM). This sample was used for examination using SANS, the 1 mm thickness being a compromise between minimisation of multiple scattering, and required intensity of scattering. The remaining slice of material, about 2 mm thick, was used for quantitative metallographic examination.

3. Experimental methods

3.1. *Small angle neutron scattering*

The small angle neutron scattering (SANS) measurements were carried out on the SANS2D small-angle scattering instrument at the ISIS Pulsed Neutron Source, Rutherford Appleton Laboratory, UK (Heenan et al., 2011). A scattering vector, Q, ranging from 0.01 to 2.8 nm^{-1} was achieved utilizing an incident wavelength range of 0.42 to 1.25 nm and employing an instrument set up of incident and scattered beam lengths of 12 m. The 1 m^2 area position sensitive detector was offset vertically by 150 mm and sideways by 200 mm. With this range of scattering vector material defects, such as carbides and cavities, up to about 300 nm in size can be measured. Fig. 1 shows the various positions in the vicinity of the crack and also in the far-field region from which SANS was measured. For each position the sample was carefully aligned so that it was located in the centre of the neutron beam. An incident beam aperture of area 3 mm × 3 mm, corresponding to a gauge volume of ~9 mm^3, was used for most positions, but an aperture of area 1.5 mm × 3 mm, giving a gauge volume of ~4.5 mm^3, was used for positions 15 to 17 in Fig. 1, closely spaced between the weld and the crack. The coordinates of all these measurement positions are given in Table 2.

Table 2. The coordinates of measurement positions using SANS and QM techniques. Here x is the distance from the crack mouth and y is the distance from the crack line, in mm.

Point ID	(x,y)	Remarks	Measurement technique	
			SANS	QM
1	(1.5, -1.5)	along the line normal to the crack 1.5 mm away from the crack mouth	✓	-
2	(1.5, -5.0)		✓	-
3	(1.5, -8.5)		✓	-
4	(4.5, -1.5)	along the line normal to the crack, 4.5 mm away from the crack mouth	✓	✓
5	(4.5, -5.0)		✓	✓
6	(4.5, -8.5)		✓	✓
7	(4.5, -12.0)		✓	-
8	(4.5, -15.5)		✓	-
9	(7.5, -1.5)	along the line normal to the crack, 7.5 mm away from the crack mouth	✓	-
10	(7.5, 1.5)		✓	-
11	(8.6, 0)	along the crack line, away from the crack tip	✓	-
12	(11.6, 0)		✓	-
13	-	Far-field	✓	-
14	-		✓	-
15	(1.5, 0.75)	along a line parallel to the crack, 0.75 mm away from the crack line	✓	-
16	(4.5, 0.75)		✓	✓
17	(4.5, 1.5)	along a line parallel to the crack, 1.5 mm away from the crack line	✓	✓

The acquisition times were about 90 min and 40 min for measurement points using the smaller and larger aperture, respectively. The neutron transmission at a few positions was also measured to enable absorption corrections to be made. The data were placed on an absolute scale by reference to the scattering from a standard sample, a solid blend of hydrogenous and perdeuterated polystyrene, in accordance with established procedures (Heenan et al., 1997). The raw scattering data set from each position was corrected for the detector efficiencies, sample transmission, empty beam scattering, and then converted to an absolute macroscopic scattering cross-section in cm^{-1} data using the instrument-specific software, Mantid (Akeroyd et al., 2013). The measured cross sections were interpreted in terms of a simple model of a 'relative' volume fraction distribution $V(D)$ of spherical scattering defects of diameter D using a maximum entropy algorithm in the Harwell routine MAXE (Potton et al., 1988). A scattering contrast factor of unity was used to obtain $V(D)$. A detailed description of the data analysis has been reported elsewhere (Hutchings, 2012). The Harwell routine MAXE has recently been improved as a user friendly routine at the Open University by reprogramming in C^{++}. In order to obtain an absolute volume fraction distribution $C(D)$ of a type of defect from $V(D)$, the nature of defects must be established and the corresponding scattering contrast factor inserted into MAXE. This identification often requires other techniques, for example from information obtained from electron microscopy on similarly aged superheater components (Jazaeri et al., 2014; Burnett et al., 2015). The distribution of carbides was here assumed to be uniform across the examined region, and cavities were assumed to be negligible in the far-field region away from

the crack where only carbides were present. The scattering from far-field positions 13 and 14 was used as a reference, and the 'relative' distribution *V(D)* subtracted from that at positions nearer the crack to isolate scattering from any cavities which might be present in vicinity of the crack. The number density of the defects $N_d(D)$, in units of m^{-3}, for carbides or cavities, can be determined on the model of a distribution of spherical defects from:

$$N_{\mathrm{d}}(D) = \frac{C(D)}{V_{sph}(D)} \qquad \text{where } V_{sph}(D) \text{ is the volume of the defect, } \frac{\pi D^3}{6} . \tag{1}$$

3.2. *Metallography*

The 2 mm thick specimen was cut further to remove a 22 mm × 22 mm sample which included the full length of the creep crack. This sample was mounted in conductive Bakelite. The sample preparation procedure included grinding to 4000 µm grit size using SiC papers, and polishing down to 0.25 µm level with diamond suspension. The final preparatory stage involved an etching procedure by immersing samples in Murakami's reagent (10 g $K_3Fe(CN)_6$, 10 g KOH, 100 ml water) for 60 s. Murakami's reagent was found to be the optimum solution for sample preparation of ex-service 316H austenitic stainless steel material as it highlights the grain boundary carbides without having a significant impact on the grain boundaries themselves (Jazaeri et al., 2014). A Zeiss Supra 55VP FEGSEM instrument was used to examine the sample in both backscattered (BS) and secondary (SE) imaging mode using an accelerating voltage of 5-10 kV and an aperture size of 30 µm. Examination of the creep induced crack showed that it is essentially intergranular in nature. It had initiated at about 1.5 mm away from the weld fusion boundary but deviated from that by an angle of about 26°. Microstructural features at a position near the crack are presented in Fig 2. Cavities (A) are mainly surrounding intergranular precipitates (B) and intragranular precipitates (C) are seen as dark spots. A recent study showed that both intergranular and intragranular precipitates are mainly $M_{23}C_6$ carbides, however the intragranular precipitates are associated with long service history and form at later stages of creep (Burnett et al., 2015). Cavities have been shown to nucleate at intergranular $M_{23}C_6$ carbides in high residual stress regions (Pommier et al., 2016).

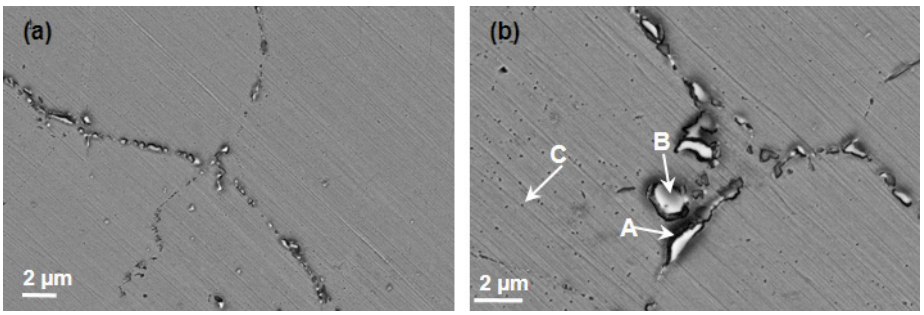

Fig. 2. Backscattered images of the microstructure near the crack a) an overview and b) close up which shows detailed microstructural features including cavities (A), intergranular carbides (B) and intragranular precipitates (C).

Quantitative Metallography (QM) was carried out in order to quantify the variation in the size and area fraction of creep cavities, e.g. dark areas surrounding bright intergranular cavities in Fig. 2. For this purpose backscattered electron images were acquired and analysed using ImageJ software. Sequential BS images were acquired at different positions normal to the crack and also along the crack line (see Table 2 and Fig. 1) using an accelerating voltage of 10 kV. At each position a series of images were analysed sampling on an average of over 135 cavities, covering a total area of over 4700 mm^2. Edge features were excluded from the analysis. Cavities up to area size of 0.07 mm^2 were measured which corresponds to about 300 nm circular diameter. This is similar to the upper threshold of the small angle measurement technique using SANS2D instrument. By defining an appropriate brightness and contrast threshold and also circularity factor $(4\pi(\text{area})/(\text{perimeter})^2)$, it is possible to separate creep cavities from both intergranular and intragranular carbides (Jazaeri et al., 2014). Here cavities can be discriminated from intragranular precipitates according to their shape difference (see Fig. 2b) using a circularity factor between 0 and 0.7.

4. Results and discussions

4.1. *SANS measurements of cavity distribution*

The fractional size distribution *C(D)* and number density $N_d(D)$ of carbides at the far-field region, measured by SANS are presented in Fig. 3. This is determined from the averaged data from the two reference positions, 13 and 14 and using the contrast factor for $M_{23}C_6$ carbides, with M largely Chromium. This size distribution of carbides at the far-field region shows two peaks at about 35 nm and 180 nm in size. This closely correlates with findings reported by (Chen et al., 2011), where a high number of the intragranular carbides with a typical diameter of 29 nm, and intergranular carbides with a typical diameter of 190 nm were found in a similar AISI Type 316H component. The far-field data were used as the reference to measure the fractional size distribution of cavities in the vicinity of the crack, as presented in Fig. 4.

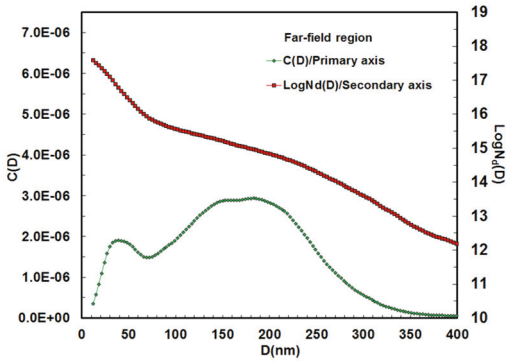

Fig. 3. Fractional size distribution *C(D)* and number density N_d *(D)* of carbides, measured by SANS, at the far-field region.

The results for positions along two lines normal to the crack, at distances of 1.5 mm and 4.5 mm away from the crack mouth, are presented in Fig. 4a, and 4b, respectively. The results for positions parallel to the crack, 1.5 mm away from the crack line and also along the crack line are shown in Fig. 4c. It is seen that the size distribution of cavities up to 300 nm can be measured by SANS2D, however above about 300 nm, the limit imposed by the lowest scattering vector, the distribution cannot be determined. As seen in Fig. 4 the cavity size distribution peaks in two regions, less than 100 nm and between 100 to 300 nm. The presence of two populations of cavities up to 300 nm in size has been observed before (Jazaeri et al., 2015) during load controlled creep tests of the same steel. In these experiments, the population of smaller cavities exhibited a pronounced increase in volume fraction distribution with increasing creep strain. Along the two lines normal to the crack, see Fig. 4a and b, there is generally an increase in the fractional size distribution of cavities approaching the crack line and also an increase along the crack line approaching the crack mouth and the crack tip (Fig. 4c). A similar systematic increase in cavitation approaching the crack line and crack mouth in the vicinity of reheat cracks in various ex-service superheater header components has been reported previously (Bouchard et al., 2004; Jazaeri et al., 2015). The number density of the two distributions of cavities as a function of distance from the crack line at 4.5 mm away from crack mouth, is presented in Fig. 4d. This has been calculated from equation 1 using an integral over *C(D)* for cavity sizes less than 100 nm and 100-300 nm in diameter. It shows that the population of cavities less than 100 nm in size have a higher number density compared with the population of larger cavities. Also, it is seen that the number density of the two populations of cavities increases approaching the crack from both sides.

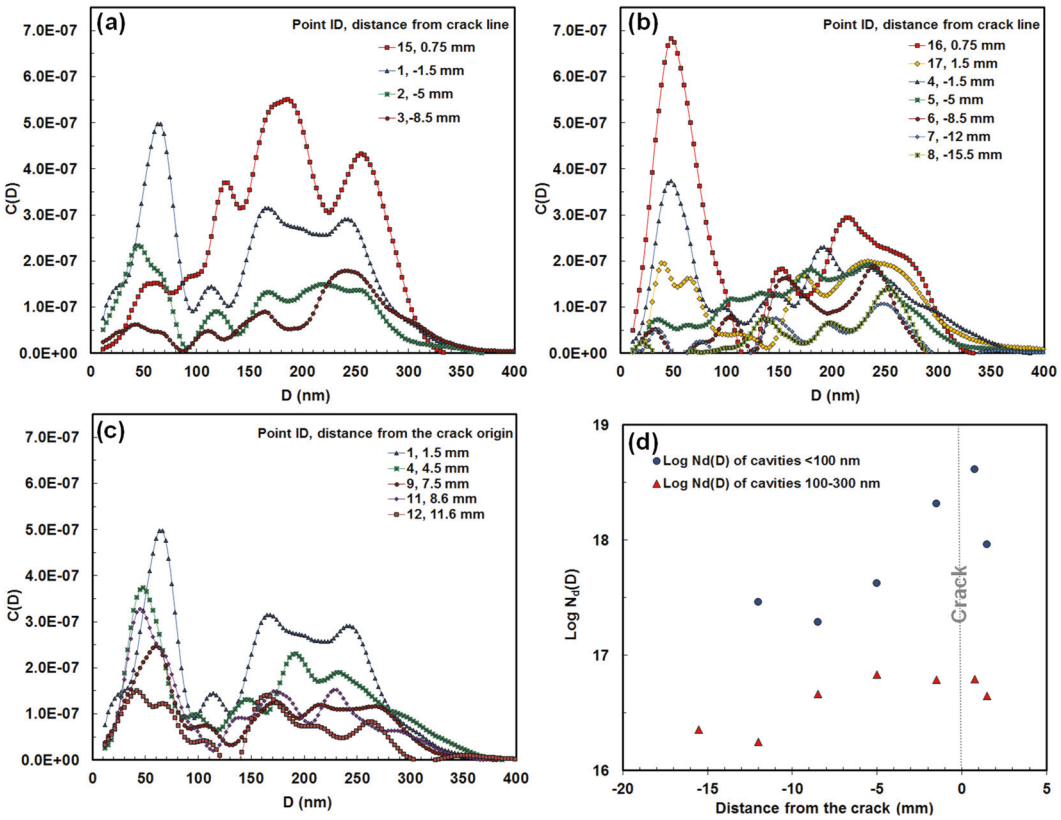

Fig. 4. Fractional size distribution *C(D)* of cavities, measured by SANS, (a) along a line normal to the crack, 1.5 mm away from the crack mouth; (b) along a line normal to the crack, 4.5 mm away from the crack mouth; (c) along a parallel line to the crack, 1.5 mm from crack and along crack line. (d) Number density of two populations of cavities as a function of distance from the crack line, measured by SANS, along a line normal to the crack, 4.5 mm away from crack mouth.

4.2. *Quantitative metallography measurement of cavities*

The variation of the area fraction (primary axis), and average area (secondary axis), of cavities measured by quantitative metallography along a line normal to the crack, 4.5 mm away from the crack mouth is shown in Fig. 5. It shows a subtle increase in area fraction of cavities (primary axis) approaching the crack line, at 0 on the abscissa. The average area of the cavities measured is about 0.0165 μm^2, corresponding to about 145 nm diameter.

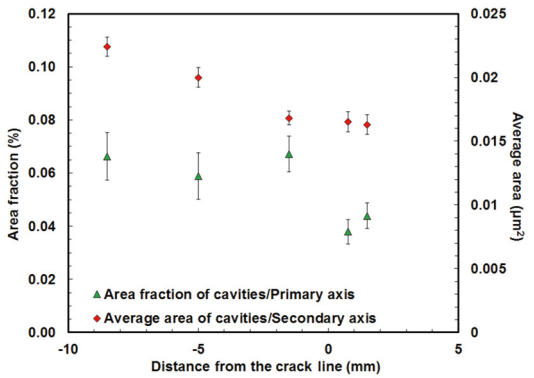

Fig. 5. Area fraction and average area of cavities, measured by QM, at positions along a line normal to the crack, 4.5 mm away from crack mouth.

4.3. *Comparison of cavity sizes measured with the two techniques*

The mean cavity size associated with the two cavity populations measured along the line normal to the crack at 4.5 mm away from crack mouth by both SANS and QM techniques is presented in Fig. 6. The mean sizes of the cavities less than 100 nm are 54 and 67 nm measured by SANS and QM respectively. So-called nanocavities of about 50 nm in size have also been observed by means of Transmission Electron Microscopy (TEM) (Pommier et al., 2016), and also by Focused Ion Beam (FIB) micro-sectioning and imaging (Chen et al., 2011). It has also been revealed that $M_{23}C_6$ carbides serve as nucleation sites for formation of these nanocavities (Pommier et al., 2016). For larger cavities up to 300 nm, the size distribution peaks at 209 and 184 nm measured by SANS and QM respectively. There is thus a good agreement between cavity sizes measured by the two techniques.

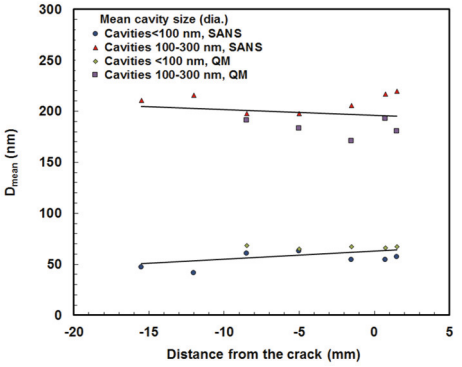

Fig. 6. Mean size of cavities measured by SANS and QM.

5. Conclusions

SANS and QM have been employed as complementary techniques to measure the size distribution of creep cavitation damage associated with a creep crack in a CT creep crack growth test specimen. The main findings of this study are:

- SANS has been successfully used to give an absolute quantitative measure of cavitation damage up to about 300 nm in size in the vicinity of the crack.
- A systematic increase in the fractional size distribution of cavities was observed at positions approaching the crack along lines normal to the crack line, and along lines parallel to the crack line approaching the crack mouth.
- These results have been compared with those from QM measurements using SEM, and a good correlation is found.
- In general two peaks in the size distribution of cavities were quantified: a population of smaller cavities of less than 100 nm size having a mean diameter of about 60 nm, and larger cavities of 100-300 nm size with a mean diameter of about 200 nm.

Acknowledgements

Funding for the research from EDF Energy and the award of neutron beam time on the SANS2D instrument at the ISIS neutron source is gratefully acknowledged. The help of Dr Sarah Rogers is acknowledged in undertaking the SANS experiments.

References

Akeroyd, F., Ansell, S., Antony, S., Arnold, O., Bekasovs, A., Bilheux, J., Borreguero, J., et al. 2013. Mantid: Manipulation and Analysis Toolkit for Instrument Data [Online]. Mantid Project. Available: http://dx.doi.org/10.5286/SOFTWARE/MANTID.

Allport, L., Dean, D. W., 2013. Boiler Lifetime and Improvement Project Creep Testing Programme: Preliminary Results from Creep Crack Growth

Tests on Type 316H Steel Heat Affected Zone, EDF Nuclear Generation Limited. E/REP/BBGB/0084/AGR/11.
Bouchard, P. J., Withers, P. J., McDonald, S. A., Heenan, R. K., 2004. Quantification of Creep Cavitation Damage Around a Crack in a Stainless Steel Pressure Vessel. Acta Materialia 52(1), 23-34.
Burnett, T. L., Geurts, R., Jazaeri, H., Northover, S. M., McDonald, S. A., Haigh, S. J., Bouchard, P. J., Withers, P. J., 2015. Multiscale Analysis of Creep Cavities and Secondary Phases in Aged AISI Type 316 Stainless Steel. Materials Science and Technology 31(5), 522–534.
Chen, B., Flewitt, P. E. J., Smith, D. J., Jones, C. P., 2011. An Improved Method to Identify Grain Boundary Creep Cavitation in 316H Austenitic Stainless Steel. Ultramicroscopy 111(5), 309-313.
Coleman, M. C., Miller, D. A., Stevens, R. A., 1998. Reheat Cracking and Strategies to Assure Integrity of Type 316 Weld Components. Integrity of High Temperature Welds London 169-179.
Duncombe, J., Wisbey, A., Ren, J., 2012. Metallography of Creep Tests from Bifurcated Weld Components, AMEC Commercial. AMEC/TS/004389/001 Issue 2.
Hales, R., 1983. Method of Creep Damage Summation Based on Accumulated Strain for the Assessment of Creep-Fatigue Endurance. Fatigue & Fracture of Engineering Materials & Structures 6, 121-135.
Heenan, R. K., Penfold, J., King, S. M., 1997. SANS at Pulsed Neutron Sources: Present and Future Prospects. Journal of Applied Crystallography 30(6), 1140-1147.
Heenan, R. K., Rogers, S. E., Turner, D., Terry, A. E., Treadgold, J., King, S. M., 2011. Small Angle Neutron Scattering using Sans2d. Neutron News 22(2), 19-21.
Hutchings, M. T., 2012. The Use of Small Angle Neutron Scattering for Mapping Creep Cavitation Damage in an Ex-Service Steam Header. The Open University, Milton Keynes, UK. OU/MatsEng/025.
Jazaeri, H., Bouchard, P. J., Hutchings, M. T., Lindner, P., 2014. Study of Creep Cavitation in Stainless Steel Weldment. Materials Science and Technology 30, 38-42.
Jazaeri, H., Bouchard, P. J., Hutchings, M. T., Mamun, A. A., Heenan, R. K., 2015. Application of Small Angle Neutron Scattering to Study Creep Cavitation in Stainless Steel Weldments. Materials Science and Technology 31, 535-539.
Jazaeri, H., Bouchard, P. J., Hutchings, M. T., Mamun, A. A., Heenan, R. K., 2015. Study of Creep Cavitation Through Creep Life. The 13th International Conference on Creep and Fracture of Engineering Materials and Structures. Toulouse, France, 167-168.
Pommier, H., Busso, E. P., Morgeneyer, T. F., Pineau, A., 2016. Intergranular Damage During Stress Relaxation in AISI 316L-type Austenitic Stainless Steels: Effect of Carbon, Nitrogen and Phosphorus Contents. Acta Materialia 103, 893-908.
Potton, J. A., Daniell, G. J., Rainford, B. D., 1988. A New Method for the Determination of Particle Size Distribution from Small-Angle Neutron Scattering Measurements. Journal of Applied Crystallography 21, 891-897.
Turski, M., Bouchard, P. J., Steuwer, A., Withers, P. J., 2008. Residual Stress Driven Creep Cracking in AISI Type 316 Stainless Steel. Acta Materialia 56(14), 3598-3612.